

A REVIEW OF GEOMETRIC MODELS AND SELF-CALIBRATION METHODS FOR TERRESTRIAL LASER SCANNERS

Revisão de modelos geométricos e de métodos de auto-calibração de equipamentos laser scanner terrestre

DEREK D. LICHTI

Department of Geomatics Engineering
Centre for Bioengineering Research and Education
The University of Calgary
2500 University Dr NW
Calgary AB Canada T2N 1N4
e-mail: ddlichti@ucalgary.ca

ABSTRACT

Terrestrial laser scanning has been shown to be an invaluable technology for engineering measurement applications such as structural deformation measurement and rockfall monitoring. In order to ensure the quality of the data captured for these and other applications, all systematic instrument errors must be properly modelled, calibrated and corrected prior to using the data in subsequent stability or deformation analyses. In one popular modelling approach, the range and angular observations from a laser scanner are augmented with additive model terms that describe the systematic errors. Self-calibration methods can then be used in order to estimate the coefficients of these models. This paper provides a review of the current state-of-the-art of terrestrial laser scanner systematic error models and self-calibration methods, supported by real-dataset examples that demonstrate the need for these processes.

Keywords: Laser Scanning; Self-calibration; Systematic Errors; Modeling.

RESUMO

Levantamento de dados a partir de terrestre laser scanner tem-se mostrado como sendo uma inestimável tecnologia para aplicações nas Engenharias de mensurações terrestres, tais como nas medidas de deformações ou de monitoramento de estruturas geológicas. Para assegurar exatidão dos resultados obtidos nessas ou em

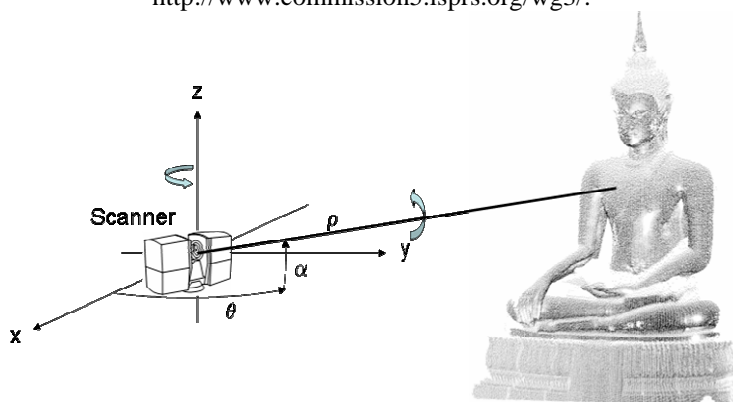
outras aplicações, os erros sistemáticos do instrumento devem ser corretamente modelados, e corrigidos, anteriormente da utilização dos dados nas análises subseqüentes de estabilidade ou de deformação. Um procedimento comum de modelagem, realizada nas observações angulares e lineares de um equipamento laser scanner, é realizado através da adição de um modelo de termos aditivos que descrevem os erros sistemáticos. Desta forma, os métodos da Auto-calibração podem então ser usados a fim estimar os coeficientes destes modelos. Este Artigo apresenta o estado da arte de modelos de correção de erros sistemáticos para equipamentos laser scanner terrestre, como também para os métodos de auto-calibração. Apresenta-se também, os resultados obtidos nos experimentos com dados reais, provando a necessidade da modelagem e correção dos erros sistemáticos.

Palavras-chave: Levantamento Laser; Auto-calibração; Erros Sistemáticos; Modelagem.

1. INTRODUCTION

Terrestrial laser scanning (TLS) instruments are active 3D imaging systems that collect a set of range (ρ) measurements to objects in equal increments of arc in the horizontal (θ) and vertical (α) planes. This process is depicted schematically in Figure 1. The resulting dataset, called a point cloud, is a sampled representation of the surface(s) within the scanner's field of view.

Figure 1 - Conceptual illustration of terrestrial laser scanning. The point cloud is part of the Golden Buddha dataset available from the ISPRS Working Group V/3 *Terrestrial Laser Scanning and 3D Imaging* at <http://www.commission5.isprs.org/wg3/>.

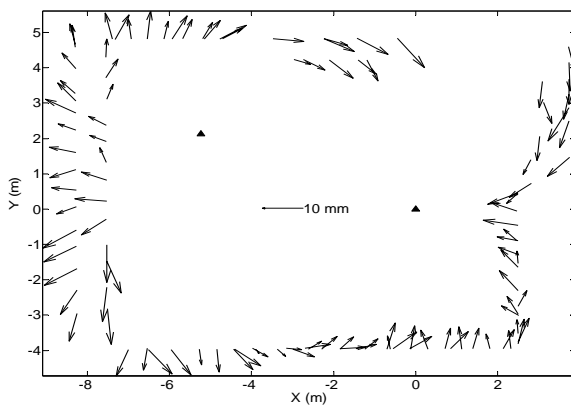


TLS instruments have found widespread use in a number of application areas, one of which is the broad area of monitoring surveys, which includes rockfall

monitoring (ABELLÁN et al., 2006; AROSIO et al., 2009), boulder stability analysis (ARMESTO et al., 2009), dam deformation measurement (ALBA et al., 2006; GONZÁLEZ-AGUILERA et al., 2008) and laboratory structural deformation measurement (GORDON and LICHTI, 2007; PARK et al., 2007; RÖNNHOLM et al., 2009). These and other precise engineering measurement applications require that all systematic instrument errors are properly modelled, calibrated and corrected in order to maximise the scanner's measurement accuracy prior to performing subsequent stability or deformation analyses with the data. The importance of these processes are underscored by RÖNNHOLM et al. (2009), who acknowledge that proper calibration would reduce residual systematic effects that are visible in their beam deflection results.

To illustrate the magnitude the effects of un-modelled systematic errors that can be encountered, consider the following example of the registration of two scans captured from different locations inside a 12 m x 9 m x 3 m room with an un-calibrated Faro 880 laser scanner. The instrument was nominally level at both positions, which were separated by 5.6 m, and the relative orientation between them was 128° in the horizontal plane. The relative rigid body transformation parameters were determined by least-squares estimation from the observation of the centres of 111 signalised targets common to both scans. As is often the case in practise, the Cartesian co-ordinates, rather than the spherical co-ordinates, were treated as observations. Figure 2 show the estimated residual vectors in plan view. Significant systematic trends are visible in the vectors, though their underlying physical causes are not immediately evident. The mean and maximum vector lengths are 6.7 mm and 11.0 mm, respectively.

Figure 2 - Residual vectors from point cloud registration of two point clouds captured by an un-calibrated Faro 880 scanner situated at the positions denoted by the triangles.



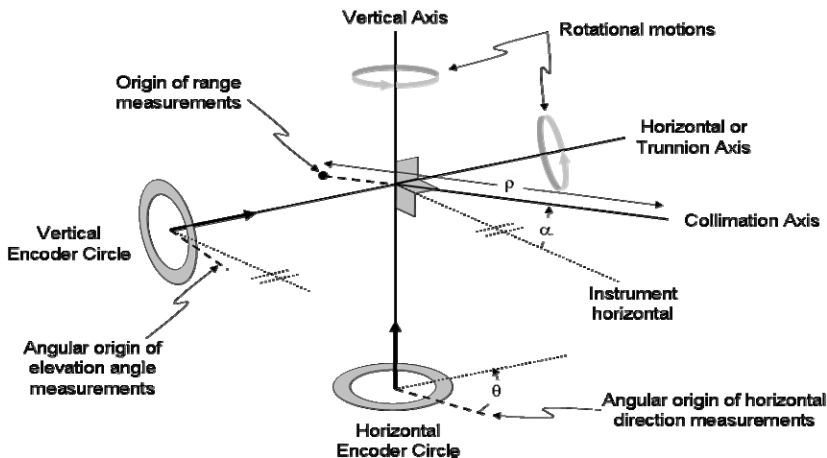
The un-modelled errors are rather obvious in this case due to the high redundancy of the registration adjustment, which in fact underscores the need for the modelling and calibration processes. In a more realistic scenario with far fewer degrees-of-freedom, un-modelled systematic errors may not be so easily visible in the registration residuals (LICHTI, 2008). Furthermore, the maximum observed elevation angle above or below the instrument's horizon was 28° in this example, which is not very large. In a real situation, the range of elevation angle observations may be much larger, i.e. up to the zenith. As will be discussed, many systematic error sources grow significantly with increasing elevation angle.

The purpose of this paper is to review the current state-of-the-art of TLS system error modelling and self-calibration. Discussion is restricted to those scanners that measure range from a few metres up to a few hundred or a few thousand metres. The review begins with a brief description of a geometric model for TLS systems, including a general discussion of TLS system operation. (A review of the details of current hardware configurations is beyond the scope of this paper.) This is followed by the primary foci of the paper: the current state-of-the-art in self-calibration methods, the relevant observation and condition equations and instrumental systematic error models.

2. TLS SYSTEM MODEL

The geometry of a TLS can be modelled in a manner similar to a total station as pictured in Figure 3.

Figure 3 - A geometric model for TLS instruments



The range to target (ρ) may be determined by either the pulse time-of-flight or the phase-difference methods, whose operation can be found in AMANN et al. (2001). In most TLS instruments, rotation of the entire instrument head about the vertical axis provides beam deflection in the horizontal plane. At each step of the horizontal motion the laser beam (assumed to be coincident with the collimation axis) is deflected in a vertical plane by rotation about the horizontal or trunnion axis. The mechanism to perform this deflection may be a nodding mirror (galvanometer) or a rotating mirror (single-facet centric or multiple-facet eccentric). The normal vectors of the planes containing the encoders, which provide the horizontal direction (θ) and elevation angle (α) measurements and are assumed to be coincident with their corresponding rotation axes, are indicated by the bold arrows.

TLS instruments can be categorised according to their architecture (e.g. STAIGER, 2003). A so-called camera scanner has narrow horizontal and vertical fields of view (e.g. 40° for both) with the beam deflection in both directions performed by dual nodding mirrors. Panoramic and hybrid scanners collect data through the full 360° horizontal range by means of a rotating scanner head, albeit in different manners. A panoramic scanner rotates about its vertical axis through a range of 180° and its vertical field of view is nearly a complete circle except for a sector of a few tens of degrees at the instrument's nadir. A hybrid scanner has a 360° horizontal rotation range, but the vertical angle deflection ranges from a few tens of degrees above nadir up to or below the zenith.

3. CALIBRATION METHODS

3.1 Individual component calibration

At least two modes of scanner calibration can be undertaken. In component calibration, the individual system components (e.g. the rangefinder and the beam deflection mechanisms) are calibrated independently under specific test conditions, sometimes using specialised facilities. One example is rangefinder calibration over an electronic distance measurement (EDM) baseline. A problem with this approach is that EDM baselines are purpose-built facilities designed for surveying equipment calibration, not for TLS systems. TLS instruments typically have much shorter unit lengths (i.e. half the modulating wavelength) than that of surveying EDMs, so the TLS periodic range errors can't be estimated.

3.2 Self-calibration methods

The premise of self-calibration methods is that all components of a TLS system are considered together as a whole. Both individual component errors (e.g. periodic rangefinder errors) and inter-component dependencies due to axis misalignments, for example, are modelled. Self-calibration methods can be

performed without recourse to special facilities; only a room with appropriate targeting (described below) is required. Network design has to be carefully considered, though, in order to ensure a strong geometric configuration that will allow the de-correlation of pertinent model variables and thereby maximise the accuracy of the estimated systematic error parameters. Network design measures are not discussed here, though; see LICHTI (2007, 2010) for details. High redundancy is also important to ensure that all systematic errors can be identified in the adjustment residuals and subsequently modelled with analytical correction functions.

3.2.1 Plane-based self-calibration

In the plane-based method of GIELSDORF et al. (2004), several point clouds are captured from different instrument locations in a room containing featureless, planar calibration panels placed at various locations and in different orientations. The point clouds are segmented into subsets of points belonging to the different panels. Each point observation vector in a subset is conditioned to lie on its corresponding planar panel and a system of least-squares normal-equations is formed and solved, subject to minimum datum constraint conditions, to simultaneously estimate the scanner position and orientation (i.e. the exterior orientation parameters), the plane parameters and the additional parameters of the systematic error models. Variants of this procedure have been proposed by BAE and LICHTI (2007), who performed system self-calibration using the walls, floor and ceiling of the room rather than specifically-placed panels, and DORNINGER et al. (2008) who focused on on-site cyclic error estimation also using planar features.

3.2.2 Point-based self-calibration

The point-based method requires several point clouds, captured from different instrument locations and in different orientations, in a room containing signalised planar targets mounted on the walls, floor and ceiling. As shown in Figure 4, the targets feature high-contrast components: e.g. a grey circle on a white background. Retro-reflective targets are not recommended as they can cause severe biases in the range measurements known as walk error (e.g., AMANN et al., 2001; LICHTI et al, 2005; PESCI and TEZA, 2008). Each target must be identified in each point cloud and its centre must be measured. Observation equations for each target centre are written and the system of normal equations is solved for the exterior orientation parameters, the target point co-ordinates and the additional parameters. Several authors have adopted this approach including LICHTI (2007, 2009, 2010) LICHTI and FRANKE (2005), LICHTI and LICHT (2006) LICHTI et al. (2007), RESHETYUK (2006, 2009), SCHNEIDER (2009) and SCHNEIDER and SCHWALBE (2008).

Figure 4 - Panoramic view of a point cloud of a calibration room for point-based self-calibration.



4. FUNCTIONAL MODELS

4.1 Point-on-plane condition

In plane-based self-calibration, the position vector of point i in scanner space j can be written in terms of the spherical observations (ρ, θ, α) as follows

$$\bar{\mathbf{p}}_{ij} = \begin{pmatrix} x_{ij} \\ y_{ij} \\ z_{ij} \end{pmatrix} = \begin{pmatrix} (\rho_{ij} - \Delta\rho + \varepsilon_{\rho_{ij}}) \cos(\alpha_{ij} - \Delta\alpha + \varepsilon_{\alpha_{ij}}) \cos(\theta_{ij} - \Delta\theta + \varepsilon_{\theta_{ij}}) \\ (\rho_{ij} - \Delta\rho + \varepsilon_{\rho_{ij}}) \cos(\alpha_{ij} - \Delta\alpha + \varepsilon_{\alpha_{ij}}) \sin(\theta_{ij} - \Delta\theta + \varepsilon_{\theta_{ij}}) \\ (\rho_{ij} - \Delta\rho + \varepsilon_{\rho_{ij}}) \sin(\alpha_{ij} - \Delta\alpha + \varepsilon_{\alpha_{ij}}) \end{pmatrix} \quad (1)$$

where $(x, y, z)_{ij}$ are the point's Cartesian, scanner-space co-ordinates ; $\Delta\rho$, $\Delta\theta$ and $\Delta\alpha$ are the respective systematic error correction models for the observations; and the ε terms are the respective random errors.

With the normal vector of target plane k defined as

$$\bar{\mathbf{n}}_k = (a_k \quad b_k \quad c_k)^T \quad (2)$$

and the orthogonal distance from the object space origin to the plane denoted as d_k , the condition equation for point i in scan j lying on plane k is given by

$$\vec{n}_k^T (\mathbf{M}_j^T \vec{p}_{ij} + \vec{P}_{c_j}) - d_k = 0 \quad (3)$$

Where,

$\vec{P}_{c_j} = (X_{c_j} \ Y_{c_j} \ Z_{c_j})^T$ is the scanner position vector; $\mathbf{M}_j = \mathbf{R}_3(\kappa_j) \mathbf{R}_2(\phi_j) \mathbf{R}_1(\omega_j)$ is the rotation matrix from object space to scanner space j ; (ω, ϕ, κ) are the rotation angles; and $\mathbf{R}_1, \mathbf{R}_2$ and \mathbf{R}_3 are the rotation matrices about the primary, secondary and tertiary rotation axes, respectively. GIELSDORF et al. (2004) parameterise the rotation in terms of the unit quaternion rather than using an Euler angle sequence is the case here.

4.2 Point-target observation equations

The point i observed from scanner location j can also be expressed in terms of range, ρ_{ij} , horizontal direction, θ_{ij} , and elevation angle, α_{ij} , observation equations

$$\rho_{ij} + \varepsilon_{\rho_{ij}} = \sqrt{x_{ij}^2 + y_{ij}^2 + z_{ij}^2} + \Delta\rho \quad (4)$$

$$\theta_{ij} + \varepsilon_{\theta_{ij}} = \arctan\left(\frac{y_{ij}}{x_{ij}}\right) + \Delta\theta \quad (5)$$

$$\alpha_{ij} + \varepsilon_{\alpha_{ij}} = \arctan\left(\frac{z_{ij}}{\sqrt{x_{ij}^2 + y_{ij}^2}}\right) + \Delta\alpha \quad (6)$$

Equations 5 and 6 are architecture-dependent. For a panoramic scanner, 180° must be added to the right-hand side of Equation 5 and the right-hand side of Equation 6 must be subtracted from 180° if the calculated horizontal direction is negative, i.e. $\theta < 0^\circ$ (LICHTI, 2010).

Scanner space is related to object space by the rigid body transformation, whose components must be substituted into the observation equations above

$$\vec{p}_{ij} = \mathbf{M}_j \{ \vec{P}_i - \vec{P}_{c_j} \} \quad (7)$$

where $\vec{P}_i = (X_i \ Y_i \ Z_i)^T$ is the vector of object-space co-ordinates for point i .

4.3 Parameter constraints

Two types of parameter constraints are considered in this sub-section. The first includes constraints necessary to prevent rank deficiencies in the normal-equations matrix due to over-parameterisation. The plane-based method requires inclusion of

one unit-length constraint equation for each plane since only two of the three direction cosines of the normal vector are independent.

$$\vec{n}_k^T \vec{n}_k - 1 = 0 \quad (8)$$

A similar constraint is needed if the quaternion rotation parameterisation is used. The length of the four-element quaternion must be constrained to be unity for each set of exterior orientation parameters.

The second type of constraint includes independently-observed, external information about the self-calibration network. The most common constraints of this type are conditions on the exterior orientation, though other types such as observed spatial distances between object points are also possible. Many constraints have been shown to be effective for the de-correlation of the additional parameters from the scanner exterior orientation and they can be easily implemented as weighted constraints. Some that have been described in recent literature are summarised below

4.3.1 Tilt angles

Inclusion of observations of the tilt angles, ω and ϕ , made by built-in inclinometers, has been shown to effectively de-correlate the vertical circle index error parameter (which is described along with other error sources in Section 4.5) from the tilt angles themselves (LICHTI, 2007) and from the scanner height, Z_c (LICHTI, 2010). The functional form of these constraints is a zero-valued observation equation, though a non-zero value is of course also possible.

$$0 + \varepsilon_{\omega_j} = \omega_j \quad (9)$$

$$0 + \varepsilon_{\phi_j} = \phi_j \quad (10)$$

4.3.2 Scanner position

Forced centring over known a position has been shown by RESHETYUK (2009) to effectively decouple the scanner position and rangefinder offset parameters. The functional form of the constraints is as follows

$$X_{c_j}^{obs} + \varepsilon_{X_{c_j}} = X_{c_j} \quad (11)$$

$$Y_{c_j}^{obs} + \varepsilon_{Y_{c_j}} = Y_{c_j} \quad (12)$$

$$Z_{c_j}^{obs} + \varepsilon_{Z_{c_j}} = Z_{c_j} \quad (13)$$

where the ‘obs’ superscript indicates the observed co-ordinates. The corresponding stochastic model for these constraints must include the uncertainties in the surveyed

co-ordinates, in the instrument centring and in the instrument height measurement (RESHETYUK, 2009).

4.3.3 Scanner orientation

Observation of the tertiary rotation angle, κ , by, say, digital compass, is necessary for effective decoupling of κ from the collimation axis error in hybrid scanner self-calibration (LICHTI, 2010). Though implementation of this constraint has not been deeply investigated, the constraint equation is given by

$$\kappa_j^{\text{obs}} + \varepsilon_{\kappa_j} = \kappa_j \quad (14)$$

4.4 Datum constraints

Regardless of the self-calibration method adopted, a TLS network has an inherent datum defect of 6. Though the network scale is implicitly defined by the range observations, the three elements of network position and three elements of network orientation must be explicitly defined. This can be accomplished by the inclusion of appropriate parameter constraints. GIELSDORF et al. (2004) adopt an ordinary minimum constraint approach by fixing the position and orientation of one scan, whereas LICHTI (2007) uses the inner constraints.

The aforementioned parameter constraints provide some datum definition information. The tilt angle observations remove the defects of rotation about the X and Y axes and the scanner orientation observation removes the defect of rotation about the Z axis. The translation defects are removed by the scanner position constraints.

4.5 Systematic error models

Instrumental systematic errors in TLS observations can be traced to deviations from the ideal system in which all axes shown in Figure 3 intersect at a common point and are mutually orthogonal. They can be modelled with additive correction terms ($\Delta\rho$, $\Delta\theta$ and $\Delta\alpha$) in the relevant observation or condition equations. The focus here is on models that describe the physical nature of the error source, though it should be noted that other approaches have been investigated. One example is MOLNÁR et al. (2009) who use a piecewise-linear range correction model.

4.5.1 Range

The systematic error model for the range observations can be expressed in terms of groups of correction terms.

$$\Delta\rho = \rho_0 + \lambda_p \rho + \Delta\rho_{\text{per}} + \Delta\rho_{\text{other}} \quad (15)$$

The first two terms, the rangefinder offset (ρ_0) and the scale error (λ_p) are considered separately since they are the most fundamental error terms. The rangefinder offset is caused by the physical offset between the range measurement origin and the scanner space origin, as illustrated in Figure 3, and/or internal electronic delays. The scale error is due to an error in the modulating wavelength in a phase-difference rangefinding system, for example. The third group, $\Delta\rho_{\text{per}}$, comprises terms to model the periodic (cyclic) range errors due to internal signal interference in phase-difference systems. These errors are modelled with sine and cosine terms and they may occur at several wavelengths. The final group, $\Delta\rho_{\text{other}}$, includes other systematic range errors with or without a readily-identifiable physical cause. They may be periodic functions of horizontal direction or elevation angle (LICHTI, 2007) or aperiodic functions (LICHTI et al., 2007).

4.5.2 Horizontal direction

The horizontal direction error model does not include a zero-order (index error) term since it is perfectly correlated with the tertiary angle κ (LICHTI, 2010), but it does include an encoder angle scale error term (λ_θ).

$$\Delta\theta = \lambda_\theta\theta + \Delta\theta_{\text{axis}} + \Delta\theta_{\text{ecc}} + \Delta\theta_{\text{orth}} + \Delta\theta_{\text{wob}} + \Delta\theta_{\text{other}} \quad (16)$$

Errors due to the non-orthogonality of TLS system axes are modelled in the $\Delta\theta_{\text{axis}}$ group. These include the non-orthogonality between the collimation and trunnion axes (the collimation axis error) and non-orthogonality between the trunnion and vertical axes (the trunnion axis error). These effects vary with the secant and the tangent of the elevation angle, respectively. The $\Delta\theta_{\text{ecc}}$ group includes errors due to the eccentricity of the collimation and the vertical axes, which varies inversely with range, as well as the eccentricity of the centre of encoder circle and the vertical axis, which is a periodic function of horizontal direction. Periodic terms due to non-orthogonality of the plane containing the encoder circle and the vertical axis comprise the $\Delta\theta_{\text{orth}}$ group. The periodic wobble of the trunnion axis is modelled by the $\Delta\theta_{\text{wob}}$ group. Finally, other empirically identified systematic error sources are lumped into the $\Delta\theta_{\text{other}}$ term.

4.5.3 Elevation angle

The elevation angle error model includes both index error (α_0) and scale error (λ_α) terms.

$$\Delta\alpha = \alpha_0 + \lambda_\alpha\alpha + \Delta\alpha_{\text{ecc}} + \Delta\alpha_{\text{orth}} + \Delta\alpha_{\text{wob}} + \Delta\alpha_{\text{other}} \quad (17)$$

The errors due to the eccentricity of the collimation and the trunnion axes, which varies inversely with range, and the periodic error due to eccentricity of the

centre of the encoder circle and the trunnion axis are grouped into $\Delta\alpha_{ecc}$. The $\Delta\alpha_{orth}$ group includes periodic terms due to the non-orthogonality of the plane containing the encoder circle and the trunnion axis. Periodic terms due to the wobble of the vertical axis are modelled with the $\Delta\alpha_{wob}$ group. Other systematic error sources are included in the $\Delta\alpha_{other}$ group.

4.5.4 Examples

In this sub-section some examples of systematic errors identified in a Faro 880 phase-difference TLS system are presented. These include two errors whose physical cause can be readily identified as well as an empirically-identified source. In all three cases, the residuals are from point-based self-calibration adjustments with the relevant systematic error terms excluded from the model for demonstration purposes. The estimated model trend curves are also superimposed on the residual plots for reference.

Pictured in Figure 5 are the range residuals from an adjustment excluding two sets of periodic errors having wavelengths of 0.6 m and 4.8 m, which are respectively equal to one-half of the shortest and median unit lengths of the Faro 880 system. Without these four terms the root mean square (RMS) value of the range residuals is 1.5 mm and there are 18 observations flagged as potential outliers by data snooping. When the appropriate model terms are added to the adjustment, the RMS drops to 1.2 mm and there are no detected outliers. The amplitudes of the sinusoidal correction terms are 1.9 mm and 1.3 mm for the short- and long-wavelength components, respectively.

The horizontal direction residuals from an adjustment excluding the trunnion axis error term are shown in Figure 6. Without this term, the RMS of horizontal direction residuals is 128" (0.036°) and there are several hundred flagged outliers in both the horizontal direction and in the elevation angle residuals. Including this term (estimated value: 277" or 0.077°) in the calibration model causes the RMS of the horizontal direction residuals to be reduced by nearly an order of magnitude to 17" (0.0047°). This example shows that the effect of the trunnion axis error on the horizontal direction observations grows rapidly as the elevation angle increases or decreases. This is also true for the collimation axis error, which varies with the secant of the elevation angle.

Figure 5 - Un-modelled periodic range errors in the range residuals from self-calibration (points) and the estimated error model trend (solid curve).

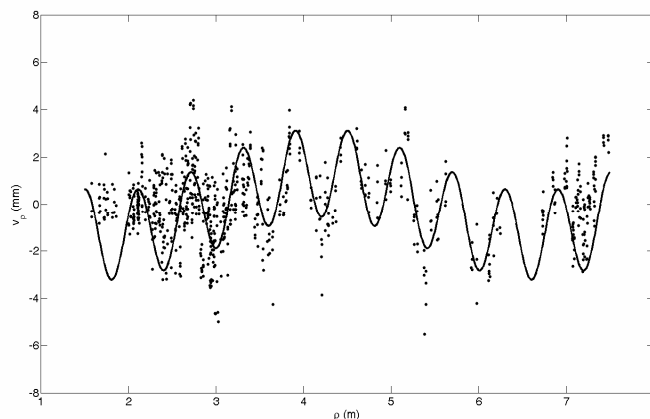
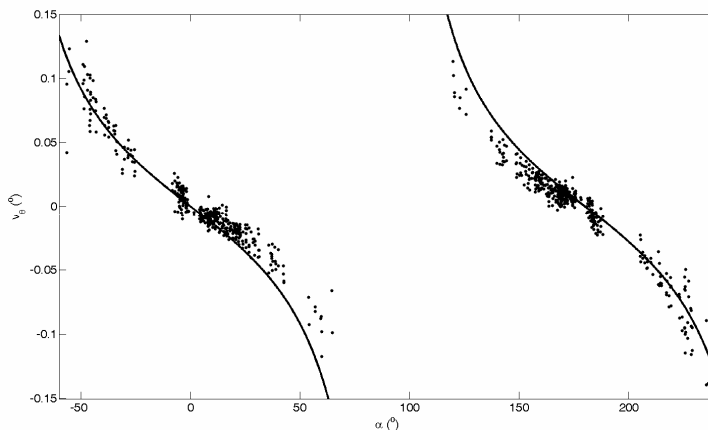


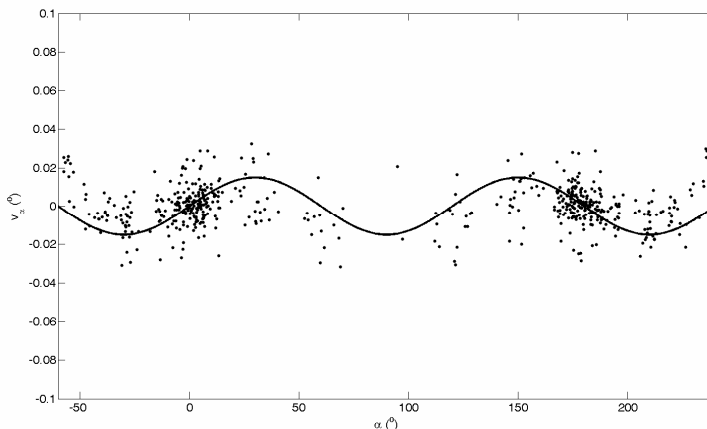
Figure 6 - Un-modelled trunnion axis error in the horizontal direction residuals from self-calibration (points) and the estimated error model trend (solid curve).



Shown in Figure 7 are the elevation angle residuals from an adjustment omitting an empirically-identified periodic error that depends on the elevation angle. The RMS of the elevation angle residuals from the adjustment excluding this single parameter from the model is 40" (0.011°) and there are 6 identified outliers. After adding the parameter (estimated magnitude: 54" or 0.015°) to the error model, the RMS falls slightly to 35" (0.010°) and no outliers are detected. Though this improvement is of a smaller proportion than the previous case, this example shows

that other systematic errors, whose physical cause is not necessarily apparent, can exist in modern TLS instruments.

Figure 7 - Un-modelled periodic error in the elevation angle residuals from self-calibration (points) and the estimated error model trend (solid curve).



5. FINAL REMARKS

Systematic TLS instrument errors can be reliably estimated using self-calibration methods. The errors can be easily modelled with additive correction terms in either the point-on-plane condition or in the observation equations. The simultaneous adjustment approach permits optimal estimation of all model variables, including the parameters of the systematic error models. Self-calibration is preferred to component calibration since all systematic errors, including those due to component misalignment errors, are considered in a complete model, not just those of the individual components themselves.

Though publication of the plane-based method preceded the point-based method, slightly more research effort has been directed at the latter. This pattern of activity is perhaps logical since the modelling approach is very intuitive, i.e. observation equations similar to those of surveying measurements are used, and many point targets can be printed from manufacturer-supplied digital template files. Increased attention to self-calibration using features like planes, cylinders and other geometric primitives found on industrial sites, for example, may develop as this approach allows for on-site calibration that circumvents the problem of instrument instability (DORRINGER et al., 2008), which has been identified as a issue (LICHTI, 2008).

ACKNOWLEDGEMENTS

This research was supported in part by the Natural Sciences and Engineering Research Council of Canada (NSERC). The author thanks Jacky Chow for reviewing drafts of this paper.

REFERENCES

- ABELLÁN, A., VILAPLANA, J.M., MARTÍNEZ, J. Application of a long-range terrestrial laser scanner to a detailed rockfall study at Vall de Núria (Eastern Pyrenees, Spain). *Engineering Geology*, 88 (3-4), 136-148, 2006.
- ALBA, M., FREGONESE, L., PRANDI, F., SCAIONI, M., VALGOI, P. Structural monitoring of a large dam by terrestrial laser scanning. *The International Archives of Photogrammetry, Remote Sensing and Spatial Information Sciences* 36 (Part 5). On CD-ROM. 2006.
- AMANN, M. C., BOSCH, T., LESCURE, M., MYLLYLÄ, R., RIOUX, M. Laser ranging: a critical review of usual techniques for distance. *Optical Engineering*, 40 (1), 10-19, 2001.
- ARMESTO, J., ORDÓÑEZ, C., ALEJANO, L., ARIAS, P. Terrestrial laser scanning used to determine the geometry of a granite boulder for stability analysis purposes. *Geomorphology*, 106 (3-4), 271-277, 2009.
- AROSIO, D., LONGONI, L., PAPINI, M., SCAIONI, M., ZANZI, L., ALBA, M. Towards rockfall forecasting through observing deformations and listening to microseismic emissions. *Natural Hazards and Earth System Sciences*, 9, 1119-1131, 2009.
- BAE, K-H., LICHTI, D.D. An on-site self-calibration method using planar targets for terrestrial laser scanners. *The International Archives of Photogrammetry, Remote Sensing and Spatial Information Sciences* 36 (Part 3/W52), 14-19, 2007.
- DORNINGER, P., NOTHEGGER, C., PFEIFER, N., MOLNÁR, G. On-the-job detection and correction of systematic cyclic distance measurement errors of terrestrial laser scanners. *Journal of Applied Geodesy*, 2 (4), 191-204, 2008.
- GIELSDORF, F., RIETDORF, A., GRUENDIG, L. A concept for the calibration of terrestrial laser scanners. *Proceedings FIG Working Week*, Athens, Greece, 22-27 May. On CD-ROM, 2004.
- GONZÁLEZ-AGUILERA, D., GÓMEZ-LAHOZ, J., SÁNCHEZ, J. A new approach for structural monitoring of large dams with a three-dimensional laser scanner. *Sensors*, 8 (9), 5866-5883, 2008.
- GORDON, S.J., LICHTI, D.D. Modeling terrestrial laser scanner data for precise structural deformation measurement. *ASCE Journal of Surveying Engineering*. 133 (2), 72-80, 2007.
- LICHTI, D.D. Modelling, calibration and analysis of an AM-CW terrestrial laser scanner. *ISPRS Journal of Photogrammetry and Remote Sensing*. 61 (5), 307-324. 2007.

- LICHTI, D.D. A method to test differences between additional parameter sets with a case study in terrestrial laser scanner self-calibration stability analysis. *ISPRS Journal of Photogrammetry and Remote Sensing*, 63 (2), 169-180, 2008.
- LICHTI, D.D. The impact of angle parameterisation on terrestrial laser scanner self-calibration. *The International Archives of Photogrammetry, Remote Sensing and Spatial Information Sciences*. 38 (Part 3/W8), 171-176, 2009.
- LICHTI, D.D. Terrestrial laser scanner self-calibration: correlation sources and their mitigation. *ISPRS Journal of Photogrammetry and Remote Sensing*. 65 (1), 93-102, 2010.
- LICHTI, D.D., FRANKE, J. Self-calibration of the iQsun 880 laser scanner. *Optical 3D Measurement Techniques VII*, Vienna, Austria, 3-5 October, pp. 112-121, 2005.
- LICHTI, D.D., GORDON, S.J., TIPDECHO, T. Error models and propagation in directly georeferenced terrestrial laser scanner networks, *ASCE Journal of Surveying Engineering*, 131 (4), 135-142, 2005.
- LICHTI, D.D., LICHT, M.G. Experiences with terrestrial laser scanner modelling and accuracy assessment. *The International Archives of Photogrammetry, Remote Sensing and Spatial Information Sciences* 36 (Part 5), 155-160, 2006.
- LICHTI, D.D., J. FRANKE AND S. BRÜSTLE. Self Calibration and Analysis of the Surphaser 25HSX 3D Scanner. *Proceedings of the 2007 FIG Working Week*, Hong Kong SAR, 13-17 May. On CD-ROM, 2007.
- MOLNÁR, G., PFEIFER, N., RESSL, C., DORNINGER, P., NOTHEGGER, C. Range calibration of terrestrial laser scanners with piecewise linear functions, *Photogrammetrie, Fernerkundung, Geoinformation*, 1, 9-21, 2009.
- PARK, H.S. LEE. H.M., ADELI, H. LEE, I. A new approach for health monitoring of structures: terrestrial laser scanning. *Computer-Aided Civil and Infrastructure Engineering*, 22 (1), 19-30, 2007.
- PESCI, A. TEZA, G. Terrestrial laser scanner and retro-reflective targets: an experiment for anomalous effects investigation. *International Journal of Remote Sensing*, 29 (19), 5749-5765, 2008.
- RESHETYUK, Y. Calibration of Terrestrial Laser Scanners Callidus 1.1, Leica HDS 3000 and Leica HDS 2500. *Survey Review*, 38 (302), 703-713, 2006.
- RESHETYUK, Y. Self-calibration and direct georeferencing in terrestrial laser scanning. *Doctoral Thesis*. Department of Transport and Economics, Division of Geodesy, Royal Institute of Technology (KTH), Stockholm. Sweden, January, 2009.
- RÖNNHOLM, P. NUIKKA, M., SUOMINEN, A., SALO, P., HYYPPÄ, H., PÖNTINEN, P., HAGGRÉN, H., VERMEER, M., PUTTONEN, J., HIRSI, H., KUKKO, A., KAARTINEN, H., HYYPPÄ, J., JAAKKOLA, A. Comparison of measurement techniques and static theory applied to concrete beam deformation. *The Photogrammetric Record*, 24 (128), 351-371, 2009.

- SCHNEIDER, D. Calibration of a Riegl LMS-Z420i based on a multi-station adjustment and a geometric model with additional parameters. *The International Archives of the Photogrammetry, Remote Sensing and Spatial Information Sciences*, 38 (Part 3/W8), 177-182, 2009.
- SCHNEIDER, D., SCHWALBE, E. Integrated processing of terrestrial laser scanner data and fisheye-camera image data, *The International Archives of the Photogrammetry, Remote Sensing and Spatial Information Sciences*, 37 (Part B5), 1037-1043, 2008.
- STAIGER, R. Terrestrial laser scanning – technology, systems and applications. In: *Proceedings of 2nd FIG Regional Conference*, Marrakech, Morocco, 2 – 5 December, 2003, <http://www.fig.net/pub/morocco/index.htm>. Last accessed: 13 January 2010.

(Invited Paper. Recebido em Janeiro de 2010).